Fracture-induced activation in mechanophore-linked, rubber toughened PMMA

Asha-Dee N. Celestine [a, d], Brett A. Beiermann [b, d], Preston A. May [c, d], Jeffrey S. Moore [c, d], Nancy R. Sottos [b, d], Scott R. White [a, d, *]

[a] Department of Aerospace Engineering, University of Illinois at Urbana-Champaign, Urbana, IL 61801, USA
[b] Department of Materials Science and Engineering, University of Illinois at Urbana-Champaign, Urbana, IL 61801, USA
[c] Department of Chemistry, University of Illinois at Urbana-Champaign, Urbana, IL 61801, USA
[d] Beckman Institute for Advanced Science and Technology, University of Illinois at Urbana-Champaign, Urbana, IL 61801, USA

ARTICLE INFO

ABSTRACT

Fracture-induced mechanochemical activation is achieved for the first time in a structural engineering polymer. Rubber toughened PMMA is lightly cross-linked (1.0 mol%) with the mechanophore spiropyran by free radical polymerization. Single Edge Notch Tension tests are performed on the spiropyran-linked material and a distinct change in color and fluorescence is detected at the crack tip, indicating the mechanochemical transformation of the spiropyran molecules. The degree of mechanophore activation is quantified via fluorescence imaging and is observed to increase with increasing crack length. The region of mechanophore activation correlates directly with the size of the plastic zone ahead of the crack tip.

© 2014 Elsevier Ltd. All rights reserved.

1. Introduction

Fracture in elastic polymers such as poly(methyl methacrylate) (PMMA) has been studied extensively using extrinsic, non-destructive techniques for the evaluation of damage, such as piezoelectric films [1], optical fibers [2,3] and both fluorescent and photoluminescent sensors [4–8]. In this paper, we explore an intrinsic method for damage evaluation by using force-activated probe molecules (mechanophores) to produce optical changes in PMMA in response to an applied mechanical force.

While earlier research in mechanochemistry focused on polymer degradation via mechanical stress [9–12], modern mechanochemistry exploits mechanical stress as the stimulus for favorable chemical reactions in polymers. Mechanochemically active polymers have been achieved through the design and synthesis of novel mechanophores that are grafted into the backbone of the polymer chain or used as cross-linkers. As force is transferred from the polymer to the mechanophore, the chemical structure of the mechanophore is altered. The reaction of various mechanophores has been investigated both in solution [12–19] and in bulk form [20–29]. Spiropyran (SP) is one of the first mechanophores studied [20] and has been used in both solution [13] and solid state experiments [20–23] to investigate this favorable mechanochemical effect.

Spiropyran undergoes a reversible electrocyclic ring opening reaction in response to tensile force, heat and UV light [13,20–23,29] (see Fig. 1). This ring opening ruptures the spiro carbon–oxygen (C–O) bond and transforms the SP molecule from the colorless spiropyran form to the highly colored, and fluorescent, merocyanine (MC) form. Mechanophore activation is also reversible by irradiating the mechanophore with visible light at room temperature. When SP is grafted into a bulk polymer the change in color and fluorescence of the polymer is a result of the mechanochemical reaction of the mechanophore and it provides a convenient and intrinsic means of sensing mechanical stress.

Potisek and co-workers first demonstrated this reaction with spiropyran-linked addition polymers subjected to ultrasonic pulsing in the solution state [13]. Davis and co-workers later showed that the SP to MC reaction can be triggered in solid state polymers [20]. They further determined that mechanophore activation only occurs when the polymer chains are attached such that force is transmitted across the spiro C–O bond. SP activation has also been demonstrated by other researchers for cross-linked PMMA under torsion [21] and linear PMMA under tension at elevated

* Corresponding author. Department of Aerospace Engineering, University of Illinois at Urbana-Champaign, 104 South Wright Street, Urbana, IL 61801, USA. Tel.: +1 217 333 1077.
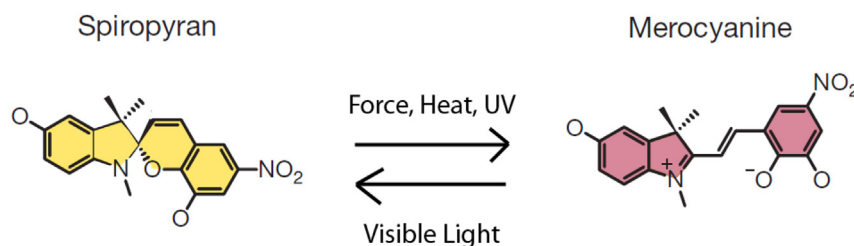E-mail address: swhite@illinois.edu (S.R. White).

Fig. 1. Transformation of spiropyran to merocyanine. The forward reaction is driven by mechanical force, heat and UV light. The reaction is reversed by illuminating with white light.

temperatures [22]. In all reported cases of force-induced SP activation in glassy bulk polymers, the SP to MC reaction occurred at the onset of yield or just beyond the yield point.

This post-yield SP activation in bulk polymers suggests that large strain at relatively high stress is a necessary condition for the mechanochemical reaction during mechanical testing. For glassy polymers such as PMMA, however, the predominant failure mechanism is crazing [30] while plastic deformation or shear yielding occurs on a much smaller scale [30–32]. Enhanced SP activation should result by increasing the degree of plastic deformation in PMMA by suppressing craze formation via compression testing [30], plasticizing the material with solvents [33], elevating the temperature [34] or incorporating core–shell rubber nanoparticles [35–41]. The incorporation of core–shell rubber nanoparticles is a well-documented strategy for increasing plastic deformation in polymers and provides not only an avenue for enhanced SP activation, but also a synergistic increase in fracture toughness.

The increased plastic deformation afforded by rubber nanoparticles leads to toughening via a three step mechanism [35,42,43]. As the material is stressed, micro-crazes develop around the nanoparticles resulting in both elastic and plastic strains on their outer surfaces [35,44]. These strains lead to cavitation within the nanoparticle as the more ductile, rubbery core deforms and detaches from the rigid shell. This cavitation triggers plastic deformation around and between nanoparticles resulting in shear yielding along the crack path [43,45,46]. Shear yielding dissipates energy and leads to macroscopic toughening of the material [35].

It is postulated that the activation energy associated with the spiropyran to merocyanine conversion is lowered upon the application of force [14,20]. This hypothesis has been tested and supported by molecular dynamics models [15,20,47] and also by macroscopic experiments and simulations [48,49]. Silberstein and co-workers were able to accurately predict the mechanical and activation response of cross-linked SP-PMMA using a potential energy surface model incorporating force modification. For the relatively low strain rates investigated (10^{-4}–10^{-2} s^{-1}), they showed that the activation of the SP was achieved by a stress-induced lowering of the activation energy barrier.

In this work, we evaluated the intrinsic damage sensing potential of spiropyran-linked PMMA via fracture-induced SP activation at low strain rates. The SP mechanophore was used as a low profile (0.05 mol%) secondary cross-linker in rubber toughened, cross-linked PMMA (see Fig. 2). Specimens were tested to failure using the Single Edge Notch Tension (SENT) fracture test. Activation of the spiropyran during fracture was assessed via optical and *in situ* fluorescence imaging. The apparent dependence of SP activation on plastic deformation reported by other researchers was also investigated by comparing the size of the SP activation zone with the size of the region of plastic deformation ahead of the crack tip.

2. Materials and methods

2.1. Material synthesis

Cross-linked PMMA (Fig. 2) with a cross-link density of 1.0 mol% was prepared by a free radical polymerization reaction. Ethylene glycol dimethacrylate (EGDMA) served as the primary cross-linker (0.95 mol%) while an acrylate functionalized spiropyran molecule [20] was used as the secondary cross-linker (0.05 mol%). Benzoyl peroxide (BPO) was used as the reaction initiator and N,N-dimethylaniline (DMA) as the activator. The cross-linked PMMA was toughened using 7.3 wt% core–shell rubber nanoparticles (Paraloid EXL 2650a) obtained from Dow Chemicals. These nanoparticles possess a butadiene-styrene (MBS) core and a PMMA shell with an average particle diameter of 250 nm.

Specimens were prepared by combining 15 mg BPO, 2.3 mg spiropyran, 75 mg MBS nanoparticles and 1 mL methyl methacrylate (MMA) in a scintillation vial. The mixture was then ultra-sonicated for 3 min (pulsed 0.2 s on, 0.2 s off) in an ice bath to uniformly disperse the core–shell rubber nanoparticles and ensure proper mixing of all components. After sonication, the vial was sealed and flushed with argon for 45 s. 16.8 μL EGDMA and 6 μL DMA were then added to the vial and the vial flushed again with argon for 45 s. The mixture was subsequently injected into a sealed glass mold of rectangular cross-section and allowed to polymerize for 24 h.

Transmission Electron Microscope (TEM) images of the polymerized material were obtained using a Philips CM200 Transmission
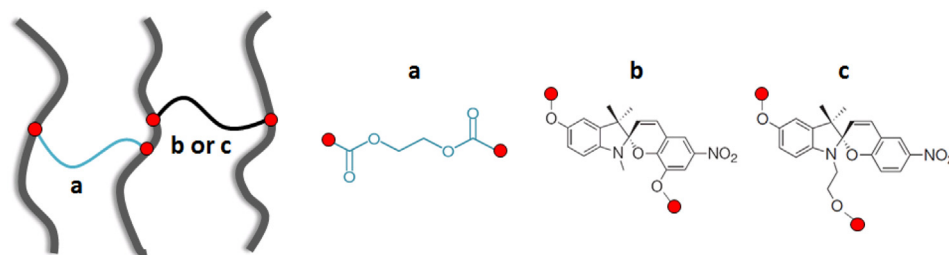

Fig. 2. PMMA polymer network with cross-linker structures (a) primary cross-linker: ethylene glycol dimethacrylate (EGDMA) (b) active SP cross-linker (c) difunctional control SP cross-linker. (Cross-link points are marked by ●).
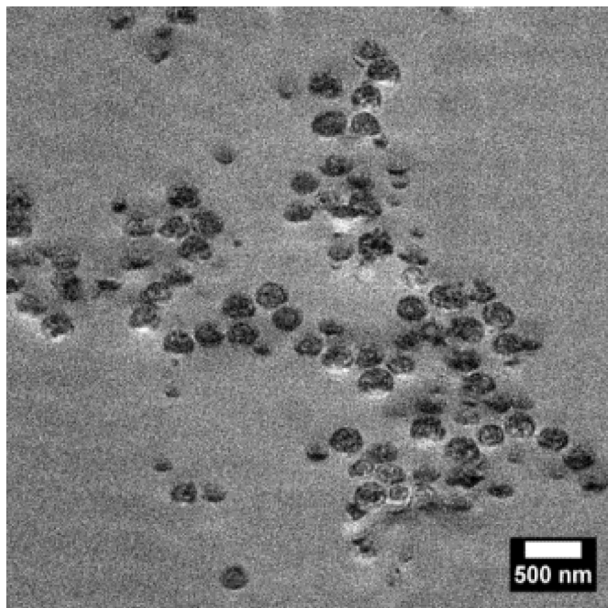
Fig. 3. Transmission electron microscope image of rubber toughened SP-PMMA showing rubber nanoparticles dispersed throughout the matrix material.

Electron Microscope. These images revealed the presence of well-dispersed rubber nanoparticles throughout the SP-PMMA material (see Fig. 3). The rubber toughened SP-PMMA material was then cut into 0.9 mm thick rectangular specimens with gage dimensions of 28 × 5 mm (see Fig. 4a). The specimens were then tabbed at both ends with heavy gage paper and placed under a 532 nm wavelength LED light for ca. 24 h to drive virtually all the mechanophores to the closed SP (colorless) form before testing.

Two types of control specimens were also synthesized using the method described above. The first control incorporated a difunctional SP mechanophore (Fig. 2, structure c) as the secondary cross-linker in which the polymer chains are not attached across the central spiro C−O bond and no force activation can occur. The second control was a rubber toughened PMMA which contained no SP mechanophore. A third type of specimen was prepared with SP-linked PMMA, but no rubber nanoparticles were included in order to isolate the effects of increased plastic deformation. Details of the synthesis recipes and material properties of all four material types can be found in the Supplementary Information. All specimens were irradiated with the 532 nm wavelength LED light for 24 h prior to testing.

2.2. Mechanical testing

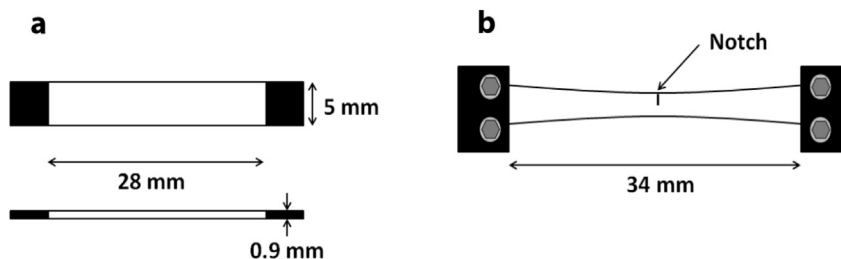Single Edge Notch Tension (SENT) tests were performed using a custom-built experimental setup that allows simultaneous
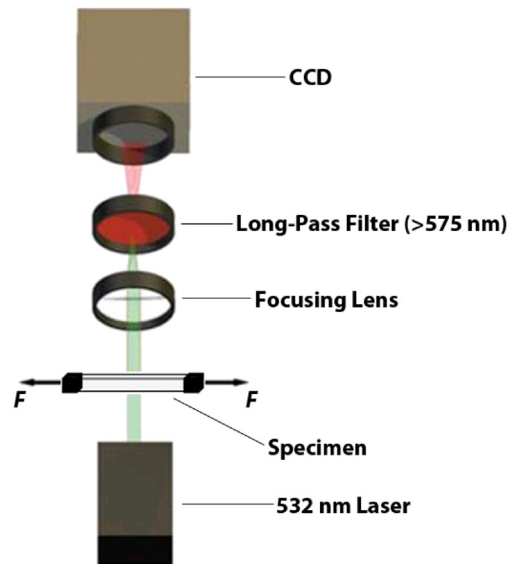

Fig. 5. Experimental setup for mechanical testing and *in situ* full field fluorescence imaging. Adapted from Ref. [22] with permission from The Royal Society of Chemistry.

mechanical testing and *in situ* full field fluorescence monitoring of the specimen gage section [22]. A screw-driven rail table in which both grips translate in opposite directions at the same rate was used to ensure that the central gage section of the specimens remained in the field of view for fluorescence imaging. Load was measured using a 220 N Honeywell Sensotech load cell. Specimens of all four material types were first prestretched to approximately 35% axial strain at a constant displacement rate of 5 μm/s in order to improve alignment and activation of the SP during SENT testing. (This displacement rate corresponds to a strain rate of 0.18×10^{-3} s^{-1}). After prestretching, the specimens were notched to a depth of approximately 1.5 mm at the center of the gage section with a razor blade yielding a normalized crack length (a/W) of ca. 0.3 (see Fig. 4b). Specimens were then irradiated with the 532 nm LED light for 24 h. After irradiation, the notched specimens were tested to failure at a displacement rate of 5 μm/s. Applied load and displacement data were collected every 0.5 s.

2.3. Fluorescence imaging

A full field fluorescence imaging setup adapted from the work of Beiermann and co-workers [22] was used to capture fluorescence images of the specimens' gage sections during SENT testing at 5 s intervals (see Fig. 5). A CrystaLaser 532 nm diode laser was used to excite the specimens at a fixed laser power of 800 μW. The emitted light from the specimens was then passed through a focusing lens and a long pass filter (>575 nm) so that only fluorescence would be

Fig. 4. Specimen geometry and configuration (a) Initial specimen dimensions (b) SENT specimen geometry after prestretch.

transmitted to a color CCD detector (AVT Stingray model F-125C). The fluorescence intensity value for each image was defined as the average red channel intensity of the CCD over the entire field of view of the specimen.

Optical images of all specimen types were also acquired after testing using a Canon EOS-1Ds Mark I SLR digital camera with a Canon 65 mm macro lens. The fracture surfaces of the rubber toughened SP-PMMA specimens were imaged with a Philips XL30 ESEM-FEG field emission environmental Scanning Electron Microscope (SEM).

2.4. Plastic zone size measurements

The length (or size) of the plastic zone ($r_{plastic}$) is the distance from the crack tip to the boundary of the plastic zone measured along the crack axis. For the specimens in this work (tested under plane strain conditions) the plastic zone size was calculated using Irwin's plastic zone correction [50]:

$$r_{plastic} = \frac{1}{3\pi}\left(\frac{K_I}{\sigma_Y}\right)^2 \tag{1}$$

where the yield stress (σ_Y) was obtained from tensile tests of pre-stretched specimens. Stress intensity factor (K_I) values were obtained from the SENT test results using [51],

$$K_I = \frac{P}{tW^{1/2}}\left[1.99\left(\frac{a}{W}\right)^{1/2} - 0.41\left(\frac{a}{W}\right)^{3/2} + 18.7\left(\frac{a}{W}\right)^{5/2} \\ - 38.48\left(\frac{a}{W}\right)^{7/2} + 53.85\left(\frac{a}{W}\right)^{9/2}\right] \tag{2}$$

where P is the applied load, a is the crack length, W is the specimen width and t is the specimen thickness.

2.5. Activation zone size measurements

Preliminary analysis of the fluorescence images acquired during SENT testing revealed approximately circular regions of SP
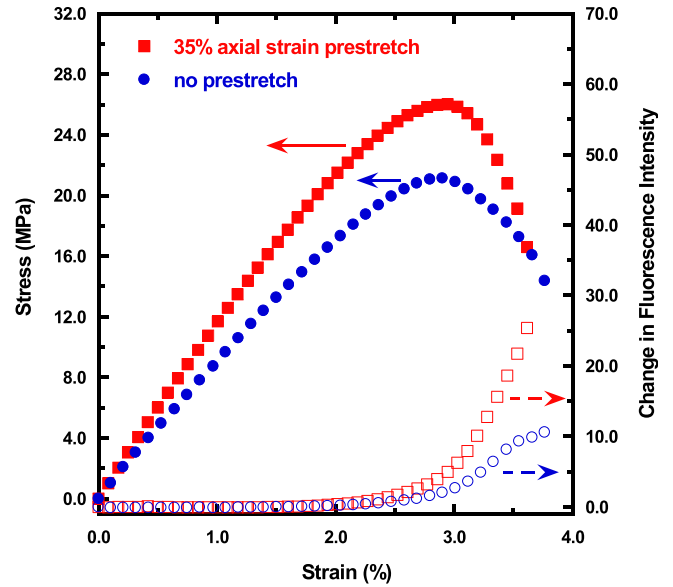

Fig. 7. Effect of prestretching on the mechanical and activation response of rubber toughened SP-PMMA during SENT testing.

activation ahead of the crack tip. Thus, three measures of activation zone size were obtained; the length and width of the activation zone and also an equivalent activation zone size obtained by assuming the activation zone is perfectly circular. Analysis of the fluorescence images was performed using the image processing software Image JA (version 1.45b). The length of the activation zone (l_{act}) in each image was obtained by performing a red channel intensity line scan from the specimen crack tip to the edge of the specimen measured along the crack propagation direction. The limit of this activation zone was taken as the location at which the red channel intensity was at least 1 standard deviation above the background intensity level. The value of l_{act} for each image was then calculated as the distance between the current crack tip and the activation zone limit (see Fig. 6a, d).
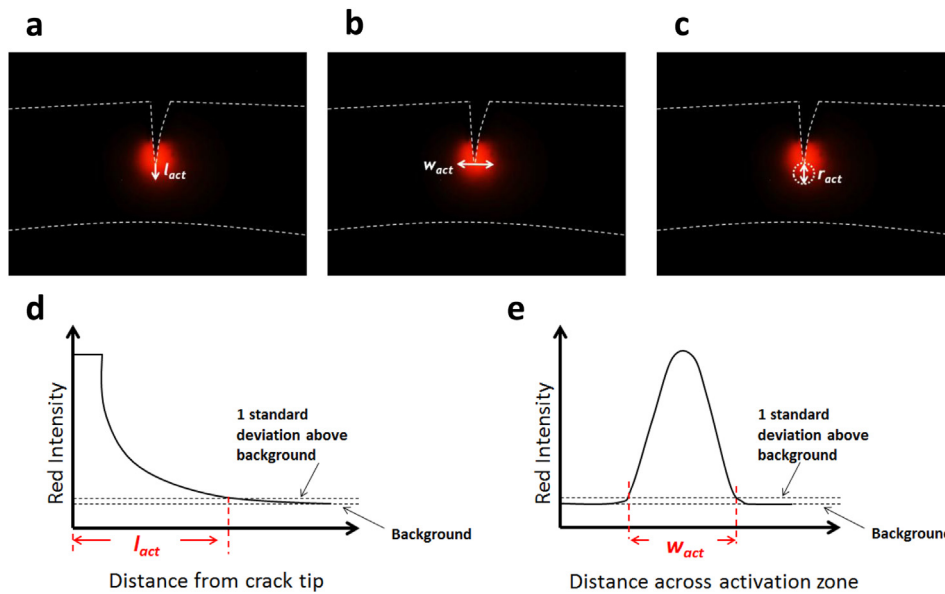

Fig. 6. Schematics of activation zone size measurements: (a) Fluorescence image during SENT testing showing activation zone length (l_{act}) definition. (b) Fluorescence image during SENT testing showing activation zone width (w_{act}) definition. (c) Fluorescence image during SENT testing showing equivalent activation zone size (r_{act}) definition. (d) Red intensity plot for activation zone length measurement. (e) Red intensity plot for activation zone width measurement. (For interpretation of the references to color in this figure legend, the reader is referred to the web version of this article.)
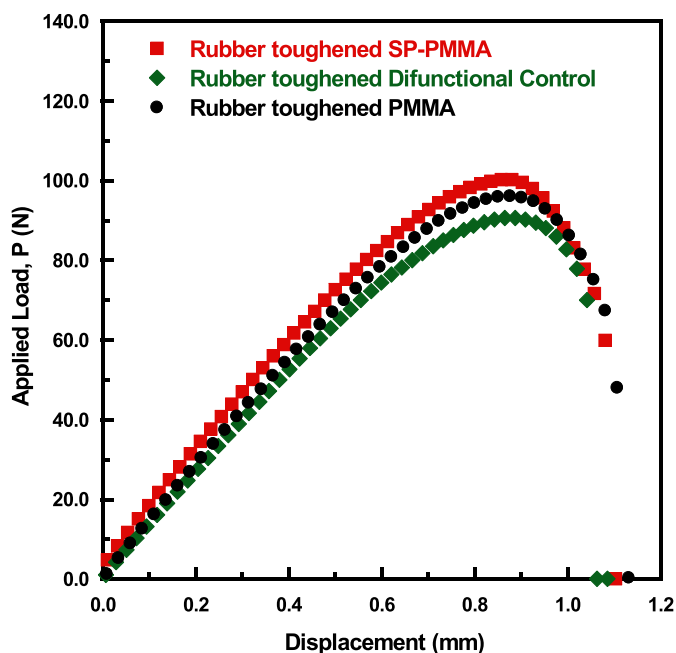
Fig. 8. Representative mechanical behavior of rubber toughened specimens during SENT tests. Specimens were tested at a displacement rate of 5 μm/s.

The width of the activation zone (w_{act}) was then determined by performing line scans perpendicular to the crack axis to find the widest region of activation. Again, the limits of activation were defined as the positions where the red channel intensity was at least 1 standard deviation above the background intensity (see Fig. 6b, e).

To obtain the equivalent activation zone size (r_{act}), the region of the image ahead of the crack tip was analyzed with a threshold set to 1 standard deviation above the background intensity. The total number of pixels above the threshold was then equated to the area of a circular activation zone with diameter r_{act} (see Fig. 6c) The various measures of activation zone size were then compared to the calculated values of $r_{plastic}$ to investigate the relationship between SP activation and plastic deformation ahead of the crack tip.

3. Results and discussion

3.1. Mechanical testing

Prestretching the specimens prior to SENT fracture testing increased the degree of mechanophore activation. This phenomenon was demonstrated in the work by Beiermann et al. where maximum fluorescence intensity was previously observed for mechanically activated SP-PMMA when the merocyanine (MC) molecules were aligned in the direction of applied tensile force [52]. The noticeable improvement in activation with prestretching (Fig. 7) is a result of chain alignment in the direction of applied force which coincides with the predominant Mode-I tensile loading of the crack tip during SENT testing. Specimens were prestretched to 35% axial strain, at a constant displacement rate of 5 μm/s, as this was the maximum applied strain to which all specimens could be consistently prestretched without material failure. The pre-stretched specimen is also observed to exhibit a higher stiffness and experiences a larger maximum stress than the specimen with no prestretch due to alignment of the polymer chains during prestretching.

Representative plots of applied load versus displacement for SENT tests of the rubber toughened specimens are depicted in Fig. 8. The SENT tests were performed at a constant displacement rate of 5 μm/s. All material types show initial linear elastic behavior up to a defined yield peak before subsequent failure. The calculated critical stress intensity factor (K_{Ic}) for the rubber toughened SP-PMMA (2.1 MPa-m$^{1/2}$) was expectedly higher than that of the non-toughened SP-PMMA (1.6 MPa-m$^{1/2}$) due to the toughening effect of the rubber nanoparticles.

Visible activation along the crack of the rubber toughened SP-PMMA was observed (see Supplementary Information). No visible activation was observed, however, for the untoughened SP-PMMA specimens or for the controls where the polymer chains were either not attached across the spiro bond or the SP molecule was absent altogether. The enhanced SP activation in the rubber toughened SP-PMMA specimens is presumably the result of increased plastic deformation afforded by the presence of the rubber nanoparticles. Examination of the fracture surface of a rubber toughened SP-PMMA specimen after SENT testing by SEM revealed a large number of voids on the surface indicative of cavitation of the rubber nanoparticles (Fig. 9a). Cavitation initiates large-scale shear yielding of the polymer [45,46,53,54] and results in improved mechanophore activation for SP-PMMA during fracture testing. An SEM image of the fracture surface of an untoughened SP-PMMA specimen obtained after SENT testing is shown in Fig. 9b. Here, the surface is relatively smooth in contrast to that of the rubber toughened SP-PMMA with no evidence of cavitation since these specimens contained no rubber nanoparticles.

3.2. Fluorescence analysis

An increase in fluorescence intensity with increasing strain was observed for the rubber toughened SP-PMMA specimen (Fig. 10a). The fluorescence images in Fig. 10b show initiation of SP activation
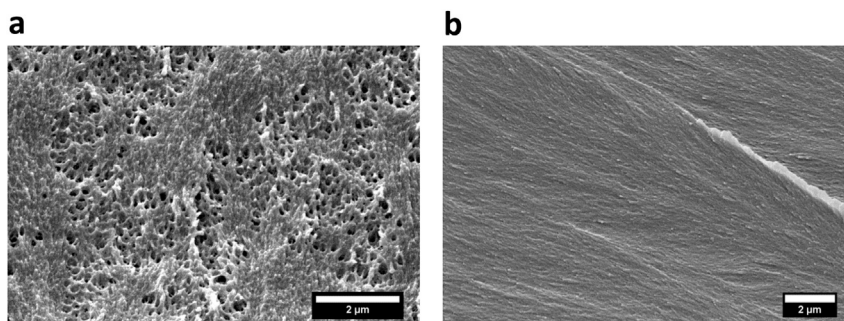

Fig. 9. Scanning electron microscope images of fracture surfaces after SENT tests (a) Fracture surface of rubber toughened SP-PMMA showing rubber nanoparticle cavitation (b) Fracture surface of untoughened SP-PMMA with no cavitation present.
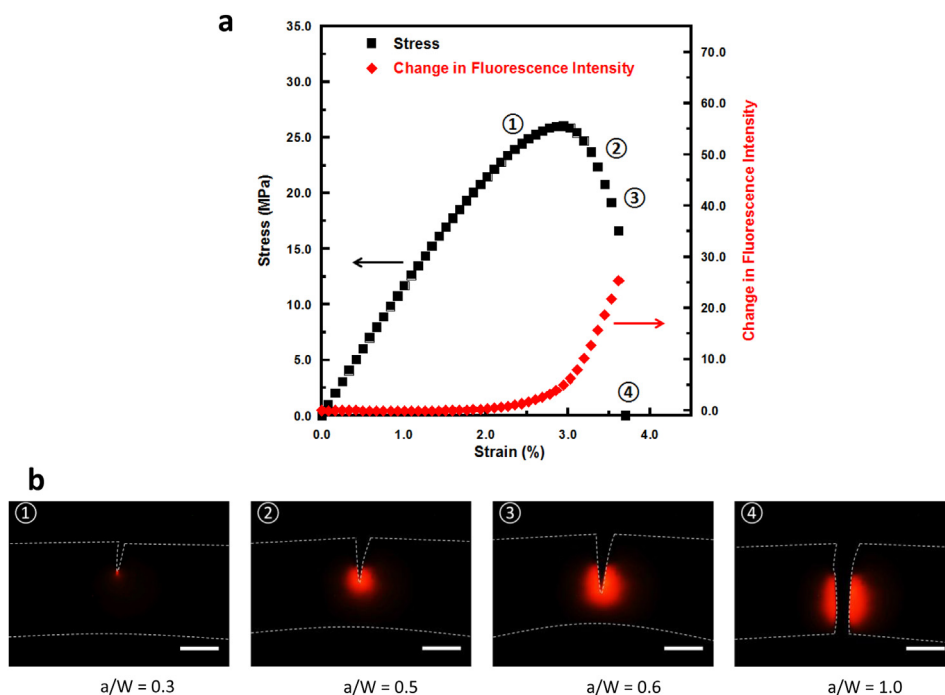
Fig. 10. SP activation response of rubber toughened SP-PMMA. (a) Stress versus strain data correlated with change in fluorescence intensity for rubber toughened SP-PMMA during SENT testing. (b) Sequence of fluorescence images of rubber toughened SP-PMMA specimen during SENT test showing evolution of fluorescence with crack propagation. The images are numbered according to their position on the stress versus strain plot in (a). *Scale bars: 2 mm.*

at the crack tip and then a growing region of fluorescence (activation zone) as crack propagation progressed. The full field fluorescence intensity also increased monotonically until complete failure of the specimen.

The change in fluorescence intensity for the rubber toughened specimens is shown in Fig. 11. Analysis of the fluorescence images of the untoughened SP-PMMA specimens (not shown) revealed a slight increase in fluoresc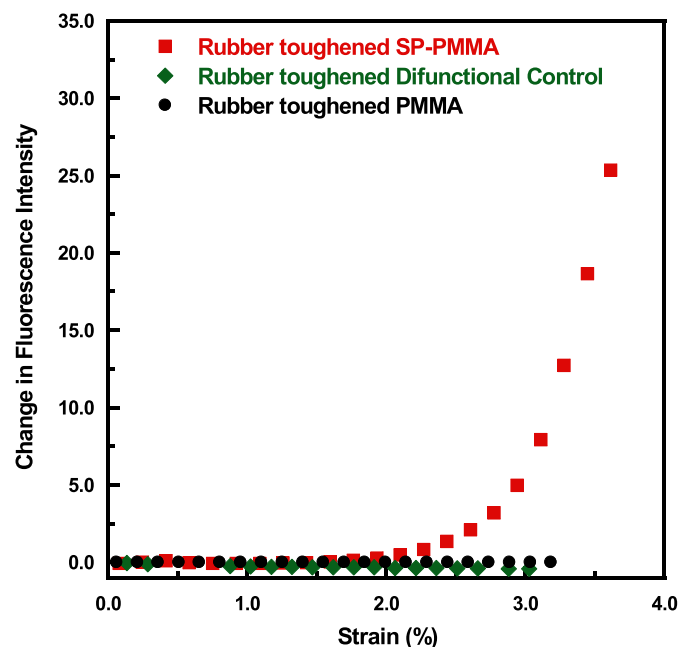ence intensity near failure suggesting a small amount of SP activation near failure. In contrast, the toughened SP-PMMA shows a large increase in fluorescence intensity that initiates beyond ca. 2% strain. This result supports the hypothesis that the inclusion of rubber nanoparticles increased plastic deformation during mechanical testing and improved the degree of mechanophore activation. No change in fluorescence intensity was observed for the rubber toughened difunctional control, confirming that the SP activation in the SP-linked specimens was the result of mechanical loading alone and not UV irradiation or heat [20]. As expected, no fluorescence signal was detected for the rubber toughened PMMA specimens since these specimens contained no SP molecules.

3.3. Activation zone size and plastic zone size analysis

The width, length and equivalent size of the activation zone were measured using the method described in the Section 2.5. Initially, all three measures of activation zone increase linearly with normalized crack length (see Fig. 12a). As the crack propagates, however, there is a noticeable plateau in the activation zone length (l_{act}) as the size of the remaining ligament in the specimen (i.e. W-a) becomes smaller until reaching the physical limit of the specimen. This trend is not observed for the activation zone width (w_{act}) because the region available for activation in that direction is not limited by specimen dimensions. The size of the equivalent activation zone (r_{act}) is at first coincident with both length and width measurements validating the assumption of a perfectly circular activation zone. With further crack growth, the equivalent activation zone size then falls between the activation zone length and width measurements. The equivalent activation zone size continues to increase with increasing crack propagation and is selected as the best representative measure of the size of the activation zone in subsequent data analysis. The effect of crack length on plastic zone size is shown in Figure SI.2 in the Supplementary Information.
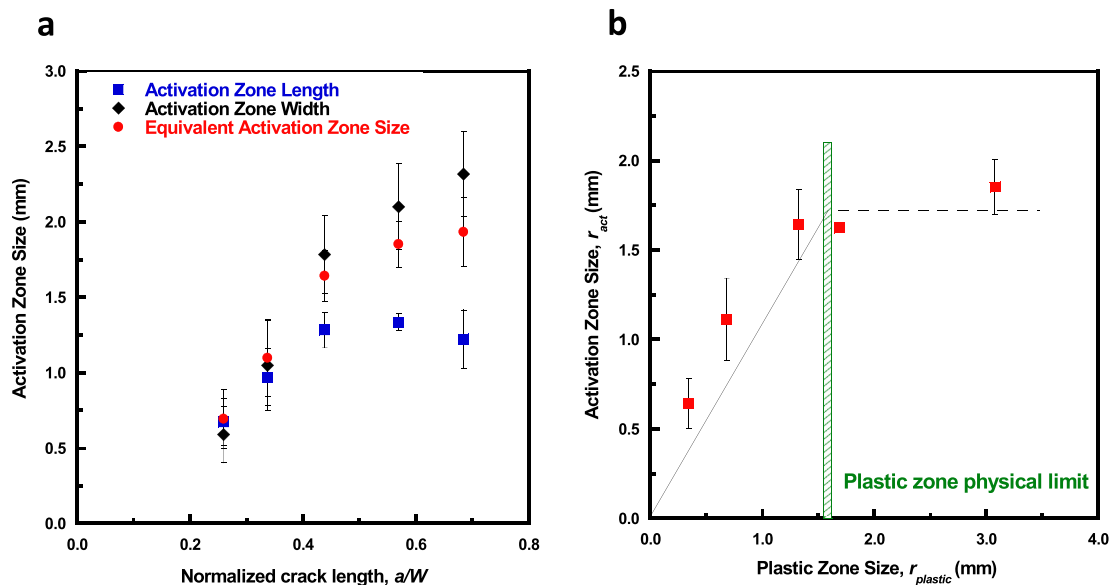

Fig. 11. Representative activation response of rubber toughened specimens during SENT test.

Fig. 12. Effect of crack growth and plastic deformation on SP activation for rubber toughened SP-PMMA. (a) Activation zone size as a function of normalized crack length. (b) Correlation of activation zone size with plastic zone size. Error bars reflect one standard deviation of the data.

A comparison of activation and plastic zone sizes reveals an initial linear increase in activation zone size with increasing plastic zone size (Fig. 12b). The slope of this linear region (first three data points) is 0.99. Two key points regarding fracture-induced mechanophore activation are drawn from these results. Firstly, SP activation occurs when there is some measure of plastic deformation in the material. This suggests that sufficient mobility of the polymer chains, which gives rise to plastic deformation, is necessary to break the spiro C–O bonds and activate the SP cross-linkers. Secondly, there is near perfect correlation between the activation zone and Irwin's plastic zone prediction demonstrating a linear relationship between the increase in plasticity and the activation of SP. Beyond the physical limit of the plastic zone imposed by specimen dimensions (shown in Fig. 12b), minimal increases in activation zone size were observed.

4. Conclusions

Fracture-induced mechanophore activation was achieved in rubber toughened PMMA cross-linked with the mechanophore spiropyran. Specimens of cross-linked SP-PMMA toughened with core–shell rubber nanoparticles were fabricated and the response of the SP mechanophore during SENT testing was examined. A custom-built experimental setup was used which allowed for simultaneous mechanical testing and *in situ* full field fluorescence imaging.

SP activation was observed during fracture and the region of activation along the crack was shown to increase in size and intensity with increasing crack length. The size of the activation zone was linearly related to the plastic zone size for moderate crack lengths, indicating an increase in SP activation with increasing plastic deformation ahead of the crack tip.

Mechanophore activation has potential for damage sensing in glassy bulk polymers and as an indicator of plastic deformation occurring ahead of the crack tip. Fracture-induced mechanophore activation may also prove to be a unique experimental method for a more detailed analysis of the fracture mechanics in rubber toughened elastic polymers. In addition to providing a measure of plastic deformation, the size and intensity of mechanophore activation can potentially be used to estimate the strain and stress fields ahead of a propagating crack.

Appendix A. Supplementary data

Supplementary data related to this article can be found at http://dx.doi.org/10.1016/j.polymer.2014.06.019.

References

[1] Zhang Y. Piezoelectric paint sensor for real-time structural health monitoring. Proc SPIE 2005;5765:1095–103.
[2] Kwon IB, Kim CG, Hong CS. Simultaneous sensing of the strain and points of failure in composite beams with an embedded fiber optic Michelson sensor. Compos Sci Technol 1997;57(12):1639–51.
[3] Zhao Y, Ansari F. Embedded fiber optic sensor for characterization of interface strains in FRP composite. Sensors Actuators A-Phys 2002;100(2–3):247–51.
[4] Generazio ER. nondestructive evaluation of ceramic and metal matrix composites for NASA's HITEMP and enabling propulsion materials programs. Cleveland, Ohio: NASA Technical Memorandum 105807; 1992.
[5] Zilberstein V, Grundy D, Weiss V, Goldfine N, Abramovici E, Newman J, et al. Early detection and monitoring of fatigue in high strength steels with MWM-arrays. Int J Fatigue 2005;27(10–12):1644–52.
[6] Cho SY, Kim JG, Chung CM. A fluorescent crack sensor based on cyclobutane-containing crosslinked polymers of tricinnamates. Sensors Actuators B-Chem 2008;134(2):822–5.
[7] Song YK, Lee KH, Hong WS, Cho SY, Yu HC, Chung CM. Fluorescence sensing of microcracks based on cycloreversion of a dimeric anthracene moiety. J Mater Chem 2012;22(4):1380–6.
[8] Löwe C, Weder C. Oligo(p-phenylene vinylene) excimers as molecular probes: deformation-induced color changes in photoluminescent polymer blends. Adv Mater 2002;14(22):1625–9.
[9] Beyer MK, Clausen-Schaumann H. Mechanochemistry: the mechanical activation of covalent bonds. Chem Rev 2005;105(8):2921–48.

[10] Porter RS, Casale A. Recent studies of polymer reactions caused by stress. Polym Eng Sci 1985;25(3):129—56.

[11] Groote R, Szyja BM, Pidko EA, Hensen EJM, Sijbesma RP. Unfolding and mechanochemical scission of supramolecular polymers containing a metal-ligand coordination bond. Macromolecules 2011;44(23):9187—95.

[12] Tennyson AG, Wiggins KM, Bielawski CW. Mechanical activation of catalysts for c-c bond forming and anionic polymerization reactions from a single macromolecular reagent. J Am Chem Soc 2010;132(46):16631—6.

[13] Potisek SL, Davis DA, Sottos NR, White SR, Moore JS. Mechanophore-linked addition polymers. J Am Chem Soc 2007;129(45):13808—9.

[14] Hickenboth CR, Moore JS, White SR, Sottos NR, Baudry J, Wilson SR. Biasing reaction pathways with mechanical force. Nature 2007;446(7134):423—7.

[15] Kryger MJ, Ong MT, Odom SA, Sottos NR, White SR, Martinez TJ, et al. Masked cyanoacrylates unveiled by mechanical force. J Am Chem Soc 2010;132(13):4558—9.

[16] Lenhardt JM, Black AL, Craig SL. gem-dichlorocyclopropanes as abundant and efficient mechanophores in polybutadiene copolymers under mechanical stress. J Am Chem Soc 2009;131(31):10818—9.

[17] Wu D, Lenhardt JM, Black AL, Akhremitchev BB, Craig SL. Molecular stress relief through a force-induced irreversible extension in polymer contour length. J Am Chem Soc 2010;132(45):15936—8.

[18] Brantley JN, Wiggins KM, Bielawski CW. Unclicking the click: mechanically facilitated 1,3-dipolar cycloreversions. Science 2011;333(6049):1606—9.

[19] May PA, Moore JS. Polymer mechanochemistry: techniques to generate molecular force via elongational flows. Chem Soc Rev 2013;42(18):7497—506.

[20] Davis DA, Hamilton A, Yang JL, Cremar LD, Van Gough D, Potisek SL, et al. Force-induced activation of covalent bonds in mechanoresponsive polymeric materials. Nature 2009;459(7243):68—72.

[21] Kingsbury CM, May PA, Davis DA, White SR, Moore JS, Sottos NR. Shear activation of mechanophore-crosslinked polymers. J Mater Chem 2011;21(23):8381—8.

[22] Beiermann BA, Davis DA, Kramer SLB, Moore JS, Sottos NR, White SR. Environmental effects on mechanochemical activation of spiropyran in linear PMMA. J Mater Chem 2011;21(23):8443—7.

[23] Lee CK, Davis DA, White SR, Moore JS, Sottos NR, Braun PV. Force-induced redistribution of a chemical equilibrium. J Am Chem Soc 2010;132(45):16107—11.

[24] Kim SJ, Reneker DH. A mechanochromic smart material. Polym Bull 1993;31(3):367—74.

[25] Nallicheri RA, Rubner MF. Investigations of the mechanochromic behavior of poly(urethane diacetylene) segmented copolymers. Macromolecules 1991;24(2):517—25.

[26] Comrie JE, Huck WTS. Exploring actuation and mechanotransduction properties of polymer brushes. Macromol Rapid Commun 2008;29(7):539—46.

[27] Foulger SH, Jiang P, Lattam AC, Smith DW, Ballato J. Mechanochromic response of poly(ethylene glycol) methacrylate hydrogel encapsulated crystalline colloidal arrays. Langmuir 2001;17(19):6023—6.

[28] Azzaroni O, Trappmann B, van Rijn P, Zhou F, Kong B, Huck WTS. Mechanically induced generation of counterions inside surface-grafted charged macromolecular films: towards enhanced mechanotransduction in artificial systems. Angew Chemie Int Ed 2006;45(44):7440—3.

[29] O'Bryan G, Wong BM, McElhanon JR. stress sensing in polycaprolactone films via an embedded photochromic compound. Acs Appl Mater Interfaces 2010;2(6):1594—600.

[30] Kinloch AJ, Young RJ. Fracture behaviour of polymers. Essex: Applied Science Publishers; 1983.

[31] Michler GH. Correlation between craze formation and mechanical-behavior of amorphous polymers. J Mater Sci 1990;25(5):2321—34.

[32] Kausch HH, Plummer CJG. The role of individual chains in polymer deformation. Polymer 1994;35(18):3848—57.

[33] Shashkov AS, Dyshlevskii YN, Voronina TA, Popova NI, Litvinov IA, Yanovskii YG, et al. Aspects of the influence of plasticizers of varied nature on the physicomechanical properties and structure of polymethylmethacrylate. Polym Sci USSR 1987;29(12):2757—64.

[34] Mizutani K. Temperature-dependence of fracture-toughness of Poly(Methyl methacrylate). J Mater Sci Lett 1987;6(8):915—6.

[35] Todo M, Takahashi K, Jar PYB, Beguelin P. Toughening mechanisms of rubber toughened PMMA. Jsme Int J Ser A-Solid Mech Mater Eng 1999;42(4):585—91.

[36] Bucknall CB. Blends containing core-shell impact modifiers - Part 1. Structure and tensile deformation mechanisms (IUPAC technical report). Pure Appl Chem 2001;73(6):897—912.

[37] Michler GH, Bucknall CB. New toughening mechanisms in rubber modified polymers. Plastics Rubber Compos 2001;30(3):110—5.

[38] Steenbrink AC, Van der Giessen E. On cavitation, post-cavitation and yield in amorphous polymer-rubber blends. J Mech Phys Solids 1999;47(4):843—76.

[39] Lovell PA, Mcdonald J, Saunders DEJ, Sherratt MN, Young RJ. Multiple-phase toughening-particle Morphology — effects on the properties of rubber-toughened Poly(Methyl methacrylate). Adv Chem Ser 1993;233:61—77.

[40] Wrotecki C, Heim P, Gaillard P. Rubber toughening of Poly(Methyl methacrylate).1. Effect of the size and hard layer composition of the rubber particles. Polym Eng Sci 1991;31(4):213—7.

[41] Cho KW, Yang JH, Park CE. The effect of rubber particle size on toughening behaviour of rubber-modified poly(methyl methacrylate) with different test methods. Polymer 1998;39(14):3073—81.

[42] Riku I, Mimura K, Tomita Y. Effect of size-dependent cavitation on micro- to macroscopic mechanical behavior of rubber-blended polymer. J Eng Mater Technol Transa ASME 2008;130(2).

[43] Lu F, Cantwell WJ, Kausch HH. The role of cavitation and debonding in the toughening of core-shell rubber modified epoxy systems. J Mater Sci 1997;32(11):3055—9.

[44] Michler GH. In situ characterization of deformation processes in polymers. J Macromol Sci Phys 2001;B40(3—4):277—96.

[45] Zairi F, Nait-Abdelaziz M, Woznica K, Gloaguen JM. Constitutive equations for the viscoplastic-damage behaviour of a rubber-modified polymer. Eur J Mech A Solids 2005;24(1):169—82.

[46] Dompas D, Groeninckx G, Isogawa M, Hasegawa T, Kadokura M. Cavitation versus debonding during deformation of rubber-modified Poly(Vinyl Chloride). Polymer 1995;36(2):437—41.

[47] Ong MT, Leiding J, Tao HL, Virshup AM, Martinez TJ. First principles dynamics and minimum energy pathways for mechanochemical ring opening of cyclobutene. J Am Chem Soc 2009;131(18):6377.

[48] Beiermann BA. Mechanical and optical characterization of force induced chemical reactions in solid state linear polymers. In: Materials Science & Engineering. University of Illinois at Urbana-Champaign; 2013.

[49] Silberstein MN, Min KM, Cremar LD, Degen CM, Martinez TJ, Aluru NR, et al. Modeling mechanophore activation within a crosslinked glassy matrix. J Appl Phys 2013;114(2).

[50] Irwin GR. Linear fracture mechanics, fracture transition, and fracture control. Eng Fract Mech 1968;1(2):241—57.

[51] Hertzberg RW. Deformation and fracture mechanics of engineering materials. Wiley; 1989.

[52] Beiermann BA, Kramer SLB, Moore JS, White SR, Sottos NR. Role of mechanophore orientation in mechanochemical reactions. Acs Macro Lett 2012;1(1):163—6.

[53] Gloaguen JM, Heim P, Gaillard P, Lefebvre JM. Plasticity of rubber-toughened Poly(Methyl methacrylate) - effect of rubber particle-size. Polymer 1992;33(22):4741—6.

[54] Lazzeri A, Bucknall CB. Applications of a dilatational yielding model to rubber-toughened polymers. Polymer 1995;36(15):2895—902.